Abstract

Motivation: Glycosylation is one of the most heterogeneous and complex post-translational modifications.
Results: These are the results for this article.

Application of Network Smoothing to Glycan LC-MS Profiling

Joshua Klein, Luis Carvalho, Joseph Zaia

November 3, 2017

1 Introduction

Glycosylation is one of the most pervasive and diverse forms of post-translational modification (Varki (2017)). Their study is of great importance for understanding broad classes of biological processes. Mass spectrometry (MS) is a powerful tool for glycan analysis (Zaia (2008)). While unseparated MS experiments using methods like MALDI provide strong signal, but cannot interpret complex mixtures Peltoniemi *et al.* (2013). An online separation method like liquid chromatography (LC) or capillary electrophoresis (CE) makes analyzing such complex samples possible, at the cost of increased analytical complexity.

There are many tools for interpreting glycan mass spectral datasets (Yu *et al.* (2013); Peltoniemi *et al.* (2013); Kronewitter *et al.* (2014); Goldberg *et al.* (2009); Maxwell *et al.* (2012); Ceroni *et al.* (2008); Frank and Schloissnig (2010)) for both unseparated and separated experimental protocols. The different types of instrumentation these programs were written to accommodate introduces different types of signal processing approaches, for example SysBioWare (Frank and Schloissnig (2010)) performs sophisticated baseline removal prior to fitting peaks, while tools like GlyQ-IQ (Kronewitter *et al.* (2014)) was written for much cleaner Fourier Transform MS (FTMS) and does not. Tools that build on the THRASH implementation from Decon2LS (Jaitly *et al.* (2009); Yu *et al.* (2013); Maxwell *et al.* (2012)) are likewise unable to deal with variable baseline noise or extreme dynamic range.

Each tool also has its own format for defining glycan structures or compositions, some even bundling a large database with their software to remove the burden from the user to build a list of candidates themselves (Yu *et al.* (2013); Kronewitter *et al.* (2014); Goldberg *et al.* (2009)) while others define methods for building glycan databases as part of the program (Maxwell *et al.* (2012); Ceroni *et al.* (2008)). Many of these tools are designed for specific glycan subclass such as N-glycans or glycosaminoglycans, limiting their vocabulary of possible monosaccharides to just those commonly found in that subclass (Yu *et al.* (2013); Kronewitter *et al.* (2014); Peltoniemi *et al.* (2013); Goldberg *et al.* (2009)). Often, these tools are tailored for analysis of a particular derivatization state, adduction conditions, or neutral loss pattern (Yu *et al.* (2013); Peltoniemi *et al.* (2013); Maxwell *et al.* (2012)).

These spectral processing and glycan library properties are reflected in the scoring function that each program uses to discriminate glycan signal from the background noise and contaminants. As observed by Goldberg *et al.* (2009), there is value in including related glycan composition identifications in how much confidence one assigns to a another glycan composition assignment. They use a method to exploit the known biosynthetic rules of N-glycans to connect peaks in a MALDI spectrum which could be assigned to a particular N-glycan by intact mass alone. Their method using the maximum weighted subgraph of the biosynthetic network in one of their three had demonstrably better performance than chance with their expert system annotation method. Kronewitter and colleagues considered a similar idea with more emphasis on handling in-source fragmentation (Kronewitter *et al.* (2014)) observed in LC-MS and LC-MS/MS experiments.

We extend this notion of a glycan family to cover more sectors of the biosynthetic landscape which we term "neighborhoods", and present an algorithm for learning the importance of each neighborhood from observed data, which can in turn be used to improve glycan composition assignment performance.

2 Methods

2.1 Glycan Hypothesis Generation

In eukaryotes, N-glycans start with a common, conserved core of **HexNAc2 Hex3**, building up to **HexNAc2 Hex9** (Stanley *et al.* (2009)). This structure is refined by sequentially removing monosaccharides and replacing them with more complex structures through a series of glycosylase and glycosyltransferase reactions, the enumeration of, which as shown in Akune *et al.* (2016), yields over a million of possible N-glycan topologies. These topologies define the geometry of the glycan, affecting the glycan's binding affinities and how the glycan may influence protein folding and accessibility, the glycan's functional aspects. The medium through which we observed glycans did not capture the full tree or graph structure of an N-glycan, so we reduced the topology to a count of each type of residue, a composition.

Starting with the core motif, we generated all combinations of monosaccharides ranging between the limits in Table 1 to build a glycan composition database, which produced 1240 distinct compositions. To perform a side-by-side comparison we also extracted the glycan list from Yu *et al.* (2013) derived from the biosynthetic rules in Krambeck and Betenbaugh (2005)

Table 1: Glycan Composition Rule Table

Monosaccharide	Lower Limit	Upper Limit	Constraints
HexNAc	2	9	
Hex	3	10	
Fuc	0	4	**HexNAc** > **Fuc**
NeuAc	0	5	(**HexNAc** − 1) > **NeuAc**

Table 2: Samples Used

Sample Name	Instrument	Derivatization	Adduction	Source
20150930-06-AGP	QTOF	Native	Formate (1)	Khatri *et al.* (2016a)
20141031-07-Phil-82	QTOF	Native	Formate (3)	Khatri *et al.* (2016a)
20141103-02-Phil-BS	QTOF	Native	Formate (3)	Khatri *et al.* (2016a)
20151002-02-IGG	QTOF	Native	Formate (2)	Khatri *et al.* (2016b)
20141128-11-Phil-82[1]	QTOF	Deutero-reduced and Permethylated	Ammonium (3)	Khatri *et al.* (2016a)
AGP-DR-Perm-glycans-1[1]	FTMS	Deutero-reduced and Permethylated	Ammonium (3)	Khatri *et al.* (2016a)
AGP-permethylated-2ul-inj-55-SLens[1]	FTMS	Reduced and Permethylated	Ammonium (3)	Khatri *et al.* (2016a)
Perm-BS-070111-04-Serum[1]	FTMS	Reduced and Permethylated	Ammonium (3)	Yu *et al.* (2013); Hu and Mechref (2012)

[1] Included MS^n Scans

with 319 compositions, and another database using all human N-glycans from GlyTouCan (Tiemeyer *et al.* (2017)) with 361 distinct compositions. As previous analysis of Influenza A virus samples detected sulfated N-glycans (Khatri *et al.* (2016a)), we also created a combinatorial database with up to one sulfate included, for a total of 2480 compositions.

2.2 LC-MS Data Preprocessing

We analyzed samples from several sources, including both QTOF and FTMS instruments as shown in Table 2. For details on sample preparation and data acquisition, please see their source citation. We converted all datasets to mzML format (Martens *et al.* (2011)) prior to analysis with Proteowizard (Kessner *et al.* (2008)) without any data transforming filters. We applied a background reduction method based upon (Kaur and O'Connor (2006)), using a window length of 2 m/z. Next, we picked peaks using a simple Gaussian model and iteratively charge state deconvoluted and deisotoped using an averagine (Senko *et al.* (1995)) formula appropriate to the molecule under study. For native glycans, the formula was **H 1.690 C 1.0 O 0.738 N 0.071**, for permethylated glycans, the formula was **H 1.819 C 1.0 O 0.431 N 0.042**. We used an iterative approach which combines aspects of the dependence graph method (Liu *et al.* (2010)) and with subtraction. All samples were processed using a minimum isotopic fit score of 20 with an isotopic strictness penalty of 2.

2.3 Chromatogram Aggregation

We clustered peaks whose neutral masses were within $\delta_{mass} = 15$ parts-per-million error (PPM) of each other. When there were multiple candidate clusters for a single peak, we used the cluster with the lowest mass error. Next, we sorted each cluster by time, creating a list of aggregated chromatograms. To account for small mass differences, we found all chromatograms which are within $\delta_{mass} = 10$ PPM of each other and which overlap in time and merge them. These mass tolerances were selected empirically, and can be adjusted as needed by the user.

2.4 Glycan Composition Matching

For each chromatogram, we searched the glycan database for compositions whose masses were within $\delta_{mass} = 10$ PPM for QTOF data, 5 PPM for FTMS data. We merged all features matching the same composition. Then, for each mass shift combination, we searched the glycan database for compositions whose neutral mass were within δ_{mass} of the observed neutral mass - mass shift combination mass, followed by another round of merging chromatograms with the same assigned composition. We reduced the data by splitting each feature where the time between sequential observation was greater than $\delta_{rt} = 0.25$ minutes and removed features with fewer than $k = 5$ data points. The same chromatogram may be given multiple assignments and designated multiple mass shifts, and chromatograms without glycan assignments may use chromatograms with glycan assignments as mass shifted components. This ambiguity information was propagated through each merge and split step.We termed these remaining assigned and unassigned chromatograms *candidate features*.

2.5 Feature Evaluation

For each candidate feature, we computed several metrics to estimate how distinguishable the observed signal was from random noise. The features are mentioned in List 1, but for more information see Section S1.

List 1: Chromatographic Feature Metrics

1. Goodness-of-fit of chromatographic peak shape to a model function (Yu and Peng (2010); Kronewitter *et al.* (2014)).
2. Goodness-of-fit of isotopic pattern to glycan composition weighted by peak abundance (Maxwell *et al.* (2012)).
3. Observed charge states with respect to glycan composition and mass.
4. Time gap between MS^1 observations detecting measuring missing peaks and interference.
5. Adduction states with respect to glycan composition and mass.

These metrics are bounded in $[0, 1)$. Any observation for which any metric was observed below 0.15 was discarded as having insufficient evidence for consideration. The *observed score* s for each candidate feature is the sum of the logit-transformation of these metrics. This produces a single value bounded in $[0, \infty)$, whose distribution we assume is asymptotically normal. $s < 8$ reflects a low confidence match, with confidence increasing as s does. As these metrics are tied to reliable detection of the the glycan by the mass spectrometer, they are dependent upon glycan abundance and sample quality and the resolution of the mass spectrometer used.

2.6 Glycan Composition Network Smoothing

Evidence for individual glycan compositions can often be enough to claim that composition had been detected. Lower abundance may score poorly in one or more features, leading to the glycan composition being discarded. Other methods have demonstrated it is advantageous to use relationships between glycans based on biosynthetic or structural rules to adjust the score of a single glycan assignment (Goldberg *et al.* (2009); Kronewitter *et al.* (2014)). We propose a method based on Laplacian Regularized Least Squares (Belkin *et al.* (2006)) to use evidence from glycan compositions related over a network to smooth it's classification of glycan composition feature matching.

2.6.1 Glycan Composition Graph

For each database of theoretical glycan compositions we create, we define each composition to be a coordinate vector in a $\mathcal{Z}^{+c}$ space where c is the number of components in any glycan composition, and represented by a node in an undirected glycan composition graph $\mathcal{G}$. Under this interpretation, we can compute the L_1-distance between two glycan compositions. For any two glycan compositions g_u, g_v, if $L_1(g_u, g_v) = 1$ we add an edge connecting g_u and g_v to $\mathcal{G}$ with weight $w = 1$.

2.6.2 Neighborhood Definition

Our definition of distance connects glycan compositions which differ by a single monosaccharide, but we can assert larger collections of glycan compositions are related. We define neighborhoods for N-glycans using intervals over monosaccharide counts defined in Table 3. These neighborhoods are arranged to span particular epitopes or biosynthetically related subtypes of N-glycans, such as sialylation state or branching pattern.

Glycan compositions may belong to zero or more neighborhoods, as there are unusual glycan compositions which do not satisfy any neighborhood's rules, and several neighborhoods intentionally overlap to express broad relationships between groups.

We define a matrix $\mathbf{A}$ as an $n \times k$ matrix where $A_{i,k}$ to be the degree to which g_i belongs kth neighborhood:

$$A_{i,k} = \frac{1}{|\text{neighborhood}_k|} \sum_{g^* \in \text{neighborhood}_k} L_1(g_i, g^*) \tag{1}$$

To reduce the impact of neighborhood size on the elements of $\mathbf{A}$, the columns of $\mathbf{A}$ are first normalized to sum to 1, and then the rows of $\mathbf{A}$ are normalized to sum to 1[1].

We assume that members of the same neighborhood will share a central tendency, τ.

[1] The stated reduction is not well tested, and the change may well be minimal because all that really happens is the weight of the column for each row is weighted by a shrinking function of column size. It may be better if we don't manipulate A at all.

Name	Bounds
High Mannose	$\mathbf{HexNAc} = 2 \wedge \mathbf{Hex} \in [3, 10] \wedge \mathbf{NeuAc} = 0$
Hybrid	$\mathbf{HexNAc} \in [2, 4] \wedge \mathbf{Hex} \in [2, 6] \wedge \mathbf{NeuAc} \in [0, 2]$
Bi-Antennary	$\mathbf{HexNAc} \in [3, 5] \wedge \mathbf{Hex} \in [3, 6] \wedge \mathbf{NeuAc} \in [1, 3]$
Asialo-Bi-Antennary	$\mathbf{HexNAc} \in [3, 5] \wedge \mathbf{Hex} \in [3, 6] \wedge \mathbf{NeuAc} \in [0, 1]$
Tri-Antennary	$\mathbf{HexNAc} \in [4, 6] \wedge \mathbf{Hex} \in [4, 7] \wedge \mathbf{NeuAc} \in [1, 4]$
Asialo-Tri-Antennary	$\mathbf{HexNAc} \in [4, 6] \wedge \mathbf{Hex} \in [4, 7] \wedge \mathbf{NeuAc} \in [0, 0]$
Tetra-Antennary	$\mathbf{HexNAc} \in [5, 7] \wedge \mathbf{Hex} \in [5, 8] \wedge \mathbf{NeuAc} \in [1, 5]$
Asialo-Tetra-Antennary	$\mathbf{HexNAc} \in [5, 7] \wedge \mathbf{Hex} \in [5, 8] \wedge \mathbf{NeuAc} \in [0, 0]$
Penta-Antennary	$\mathbf{HexNAc} \in [6, 8] \wedge \mathbf{Hex} \in [6, 9] \wedge \mathbf{NeuAc} \in [1, 5]$
Asialo-Penta-Antennary	$\mathbf{HexNAc} \in [6, 8] \wedge \mathbf{Hex} \in [6, 9] \wedge \mathbf{NeuAc} \in [0, 0]$
Hexa-Antennary	$\mathbf{HexNAc} \in [7, 9] \wedge \mathbf{Hex} \in [7, 10] \wedge \mathbf{NeuAc} \in [1, 6]$
Asialo-Hexa-Antennary	$\mathbf{HexNAc} \in [7, 9] \wedge \mathbf{Hex} \in [7, 10] \wedge \mathbf{NeuAc} \in [0, 0]$
Hepta-Antennary	$\mathbf{HexNAc} \in [8, 10] \wedge \mathbf{Hex} \in [8, 11] \wedge \mathbf{NeuAc} \in [1, 7]$
Asialo-Hepta-Antennary	$\mathbf{HexNAc} \in [8, 10] \wedge \mathbf{Hex} \in [8, 11] \wedge \mathbf{NeuAc} \in [0, 0]$

Table 3: N-Glycan Neighborhoods

2.6.3 Laplacian Regularization

We combine the observed score $\mathbf{s}$ and the structure of $\mathcal{G}$ to estimate a smoothed score ϕ that combines the evidence for each individual glycan composition as well as its relatives. As $\mathbf{s}$ is the size of the set of observed glycan composition p while ϕ is of size n, we partition ϕ into a block vector $\begin{bmatrix}\phi_o \\ \phi_m\end{bmatrix}$ with dimensions $\begin{bmatrix}p \\ n-p\end{bmatrix}$.

Let $\mathbf{L}$ be the weighted Laplacian matrix of $\mathcal{G}$, which is an $n \times n$ matrix. To ensure $\mathbf{L}$ is invertible, we add $\mathbf{I}_n$ to $\mathbf{L}$. We partition $\mathbf{L}$ into blocks $\begin{bmatrix}\mathbf{L_{oo}} & \mathbf{L_{om}} \\ \mathbf{L_{mo}} & \mathbf{L_{mm}}\end{bmatrix}$. We also partition $\mathbf{A}$ into $\begin{bmatrix}\mathbf{A}_o \\ \mathbf{A}_m\end{bmatrix}$ and $\tau_o = \mathbf{A}_o\tau$, $\tau_m = \mathbf{A}_m\tau$.

We find the ϕ that minimizes the expression

$$\mathcal{S}(\mathbf{L}, \phi, \tau) = \begin{bmatrix}\phi_o - \tau_o, & \phi_m - \tau_m\end{bmatrix} \begin{bmatrix}\mathbf{L_{oo}} & \mathbf{L_{om}} \\ \mathbf{L_{mo}} & \mathbf{L_{mm}}\end{bmatrix} \begin{bmatrix}\phi_o - \tau_o \\ \phi_m - \tau_m\end{bmatrix} \tag{2}$$

$$\ell = (\mathbf{s} - \phi_\mathbf{o})^t(\mathbf{s} - \phi_\mathbf{o}) + \lambda\mathcal{S}(\mathbf{L}, \phi, \tau) \tag{3}$$

where λ controls how much weight is placed on the network structure and τ.

To obtain the optimal ϕ, we take the partial derivative of ℓ w.r.t ϕ_m

$$0 = \frac{\partial \ell}{\partial \phi_m}\left((\mathbf{s} - \phi_\mathbf{o})^t(\mathbf{s} - \phi_\mathbf{o}) + \lambda\mathcal{S}(\mathbf{L}, \phi, \tau)\right) \tag{4}$$

$$\hat{\phi}_m = -\mathbf{L_{mm}}^{-1}\mathbf{L_{mo}}(\phi_o - \tau_o) + \tau_m \tag{5}$$

and w.r.t. ϕ_o

$$0 = \frac{\partial \ell}{\partial \phi_o}\left((\mathbf{s} - \phi_\mathbf{o})^t(\mathbf{s} - \phi_\mathbf{o}) + \lambda\mathcal{G}(\mathbf{L}, \phi, \tau)\right) \tag{6}$$

$$\hat{\phi}_o = \left[\mathbf{I} + \lambda\left(\mathbf{L_{oo}} - \mathbf{L_{om}}\mathbf{L_{mm}^{-1}}\mathbf{L_{mo}}\right)\right]^{-1}(\mathbf{s} - \tau_o) + \tau_o \tag{7}$$

To use this method, we must provide values for λ and τ. While these values could be chosen based on the expectations of the user for a given experiment, we provide an algorithm for selecting their values in Section S 4. These methods use the topology of the glycan composition graph and the distribution of observed scores, and cannot fully capture boundary cases or related but disconnected parts of the graph.

3 Results

The performance of our algorithm is demonstrated on *20141103-02-Phil-BS* and *Perm-BS-070111-04-Serum*. Please refer to section S5 for all other datasets. For each comparison, the unregularized case is not smoothed, effectively $\lambda = 0$, the partially regularized case uses the grid search fitted values of τ but uses a fixed $\lambda = 0.2$, and the fully regularized case uses the grid search fitted values of both τ and λ.

Neighborhood τ	Phil-BS			Serum		
	Combinatorial + Sulfate	glySpace	Krambeck	Combinatorial	glySpace	Krambeck
high-mannose	18.010	15.061	17.001	20.148	19.392	19.720
hybrid	13.378	12.435	13.700	19.889	18.610	20.056
bi-antennary	0.000	0.000	0.000	16.654	16.826	17.594
asialo-bi-antennary	14.135	10.916	12.913	22.221	21.563	21.827
tri-antennary	0.000	0.000	0.000	24.600	19.605	23.644
asialo-tri-antennary	14.476	6.565	10.823	20.474	21.128	19.764
tetra-antennary	0.000	0.000	0.000	18.630	18.542	17.675
asialo-tetra-antennary	14.351	4.842	6.186	4.118	7.180	2.568
penta-antennary	0.000	0.000	0.000	12.822	15.035	11.681
asialo-penta-antennary	11.582	1.255	4.892	0.000	0.000	0.000
hexa-antennary	0.000	0.000	0.000	0.000	0.000	0.000
asialo-hexa-antennary	11.089	3.883	6.612	0.000	0.000	0.000
hepta-antennary	0.000	0.000	0.000	0.000	0.000	0.000
asialo-hepta-antennary	3.120	1.529	1.351	0.000	0.000	0.000
$\hat{\lambda}$	0.99	0.69	0.99	0.99	0.99	0.99
$\hat{\gamma}$	11.39	14.60	14.42	19.32	18.42	20.67

Table 4: Estimated values of smoothing parameters τ, λ, and γ for each dataset and database

Figure 1: Chromatogram Assignments and Quantification for *20141103-02-Phil-BS* Using the *Combinatorial + Sulfate* database.

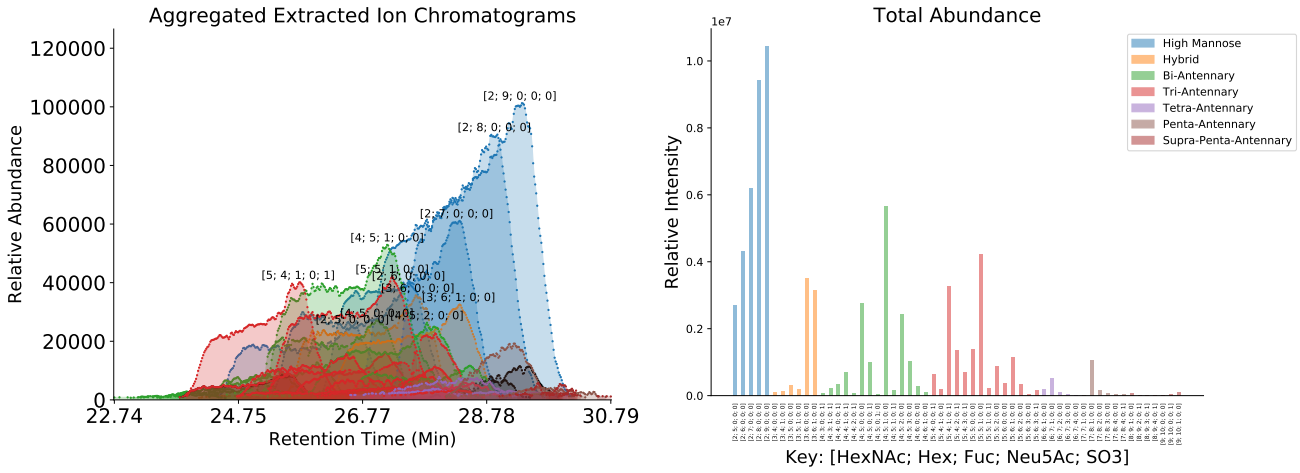

3.1 Chromatogram Assignment Performance for *20141103-02-Phil-BS*

The fitted parameters for the network constructed for *20141103-02-Phil-BS* are shown in Table 4. The assigned chromatograms are shown in Figure 1. We observe up to seven branch structures in this sample, consistent with these N-glycans being derived from an avian context (Stanley *et al.* (2009); Khatri *et al.* (2016a)).

The comparison of assignment performance with differing degrees of smoothing for each database are shown in Figure 2 and Table 5. We observed the greatest number of assignments using the combinatorial database including sulfate.

3.2 Chromatogram Assignment Performance for *Perm-BS-070111-04-Serum*

The fitted parameters for the network constructed for *Perm-BS-070111-04-Serum* are shown in Table 4. The assigned chromatograms are shown in Figure 3.

The comparison of assignment performance with differing degrees of smoothing is shown in Figure 4. We observe the greatest number of total true identifications using the partially regularized Combinatorial database. However, the Combinatorial database also has many more false positives, with a ROC AUC of 0.817. These false positives do not appear in the biosynthetically constraind Krambeck database which maximizes its ROC AUC in the partially regularized condition at 0.883. After removing all ambiguous matches, the Krambeck database also has nearly the same number of true matches as the Combinatorial database.

Figure 2: Performance Comparison with and without Network Smoothing for *20141103-02-Phil-BS*

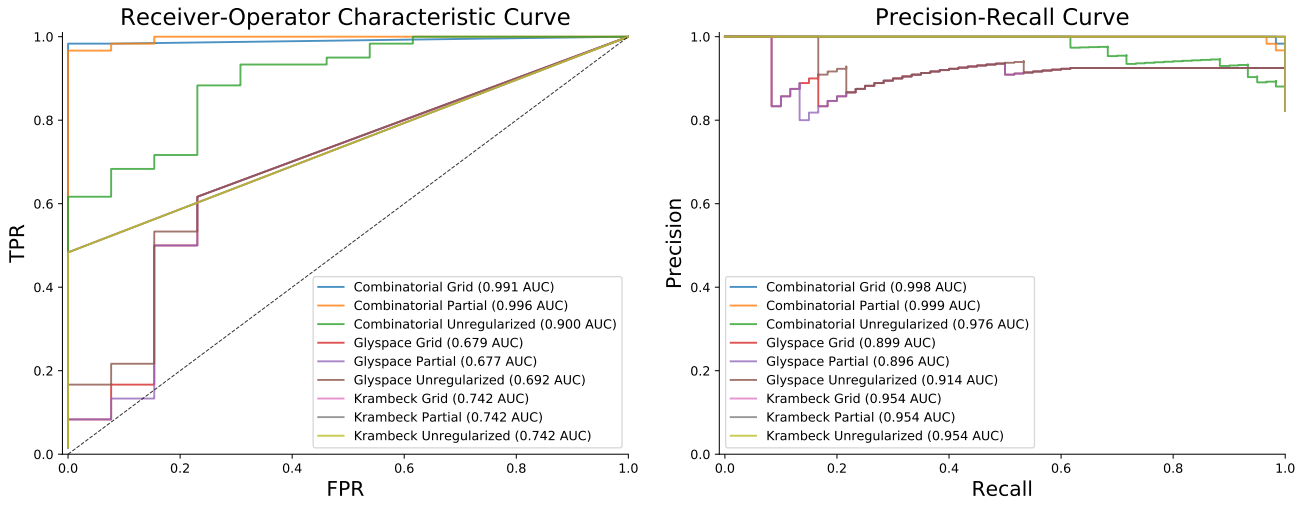

Name	ROC AUC	True Matches [1]
Combinatorial Unregularized	0.9	56
Combinatorial Partial	0.996	57
Combinatorial Grid	0.991	57
GlySpace Unregularized	0.692	37
GlySpace Partial	0.677	36
GlySpace Grid	0.679	36
Krambeck Unregularized	0.742	28
Krambeck Partial	0.742	28
Krambeck Grid	0.742	28
Khatri *et al.* (2016a)	-	46

[1] Selected at $\phi_o > 5.0$

Table 5: Performance Comparison for *20141103-02-Phil-BS*

4 Discussion

We demonstrated that this regularization method improved the sensitivity and specificity of glycan composition assignment for LC-MS based experiments. The method used similar assumptions about the importance of common substructural elements of *N*-glycans to Goldberg *et al.* (2009), but we extend this concept with the addition of a procedure for learning the relationship strengths and use broader groups of structures.

The experimental results from the original analysis of *20141103-02-Phil-BS* and *20141031-07-Phil-82* 82 demonstrated that while both strains expressed predominantly high-mannose glycosylation, *20141103-02-Phil-BS* expressed more larger complex-type structures (Khatri *et al.* (2016a)). In our findings shown in Figure 1, we recapitulate these results while reducing the number of false assignments, Table 5. There are substantial differences in both the mass spectral processing and scoring schemes which contribute to these results, but the regularization procedure is responsible for recovering many low abundance features from this comparison. As these samples are derived from chicken eggs, we have observed larger branching patterns than are observed in normal mammalian tissue (Stanley *et al.* (2009)). There is evidence for this in the *20141103-02-Phil-BS* with **HexNAc9 Hex10**-based compositions suggesting a seven branch pattern, though this cannot be determined without high quality MS^ndata. The τ fit for Phil-BS (shown) and Phil-82 (supplement) have smaller values in the neighborhoods of their largest glycan compositions as these features tended to be low in abundance and not high scoring in their own right, but were partially supported by the overlap with the next largest neighborhood, as expected. We observed the best performance with the *Combinatorial + Sulfate* database, which produced more than half-again as many true matches than the other two databases. It produced several false matches as well, but the smoothing process removed these while boosting the score of other low abundance matches which were consistent with higher scoring matches.

The Krambeck database performed identically in all smoothing conditions as it was only able to match the common species, not including cases that were multiply fucosylated or sulfated. It had no false matches ranked alongside its true matches and smoothing could not change its performance. The glySpace-derived database produced more true matches, but had a higher false positive rate because the source was under-annotated, with glycans like G13181ZZ being annotated as human-derived despite it containing a xylose, and a lower true positive rate because it was incomplete, lacking many of the

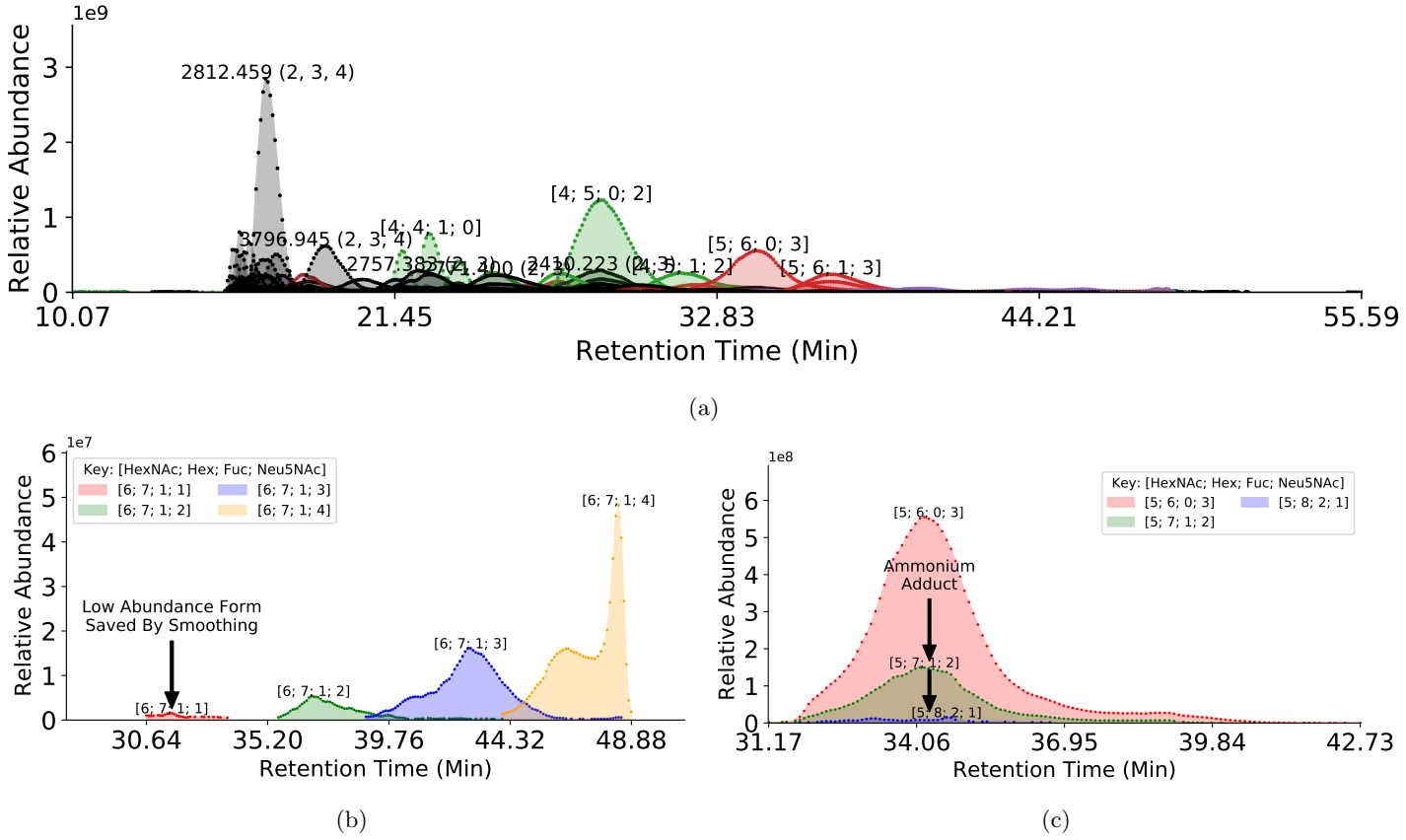

Figure 3: Chromatogram Assignments for *Perm-BS-070111-04-Serum* (a) Features Assigned After Grid Regularization of *Perm-BS-070111-04-Serum* (b) Low scoring features which may be discarded based on individual evidence alone may be more reasonable to accept given evidence from related composition, such as our network smoothing method (c) This sample contains heavy ammonium adduction which introduces ambiguity in intact mass based assignments

multiply-fucosylated large complex type species. This lead to a smaller value of $\hat{\lambda}$ (0.69), combined with a lack of contributers to the spanned components of τ to less gain from smoothing at a fixed score threshold.

As we show in Figure 4, regularization improves the predictive performance of the identification algorithm on *Perm-BS-070111-04-Serum* for all databases. We reproduce the majority of the glycan assignments from Yu *et al.* (2013), but the ambiguity caused by ammonium adduction as shown in Figure 3c makes a direct comparison of composition assignment lists difficult. Our algorithm requires a minimum amount of MS1 information in order to compute a score, which some of the assignments in the original published results do not possess, which are omitted from the count in Table 6. After accounting for ambiguity, we were able to assign all of the compositions previously reported using the Krambeck database, which was used by Yu *et al.* (2013), and with the combinatorial database. The glySpace-derived database did not contain all of these compositions, but performed competitively with the combinatorial database's ROC AUC. The combinatorial database contained a small number of glycan compositions which were not in Krambeck but which were consistent with other glycan compositions observed nearby in retention time. The combinatorial database also benefited most substantially from smoothing, discarding many false positives while retaining many more true positives at the same false positive rate compared to the other databases. These invalid glycan compositions can match LC-MS features at any point in the elution profile, though in this dataset the majority of these matches appear to be in the time range between 10 and 22 minutes, and similar glycan compositions that are biosynthetically valid elute later on in the experiment. Therefore a for a retention-time aware approach to evaluating glycan composition assignments, as described in Hu *et al.* (2016) could also be useful, but this is likely dependent upon the experimental workup and separation technique used.

While the biosynthetically constrained Krambeck database performed better on *Perm-BS-070111-04-Serum*, it did not contain all of the reasonably assignable glycan compositions, and it performed poorly on *20141103-02-Phil-BS* with a false negative rate of 50% compared to the combinatorial database. This is because the necessary enzymatic pathways were either not considered in the original authors' model because either the enzyme was excluded for simplicity (Krambeck *et al.* (2009)) or because the particular enzymes used were not within the scope of the model used (Spiro and Spiro (2000); Ichimiya *et al.* (2014)). This highlights the importance of selecting a good reference database, though a post-processing step such as the we described here can help mitigate using too large a database, but not a too small one.

In this work, we used the same network neighborhood imposed over different underlying sets of composition nodes, and the connectivity of those networks did not take into account the biosynthetic process. It may be possible to obtain

Figure 4: Performance Comparison with and without Network Smoothing for *Perm-BS-070111-04-Serum*

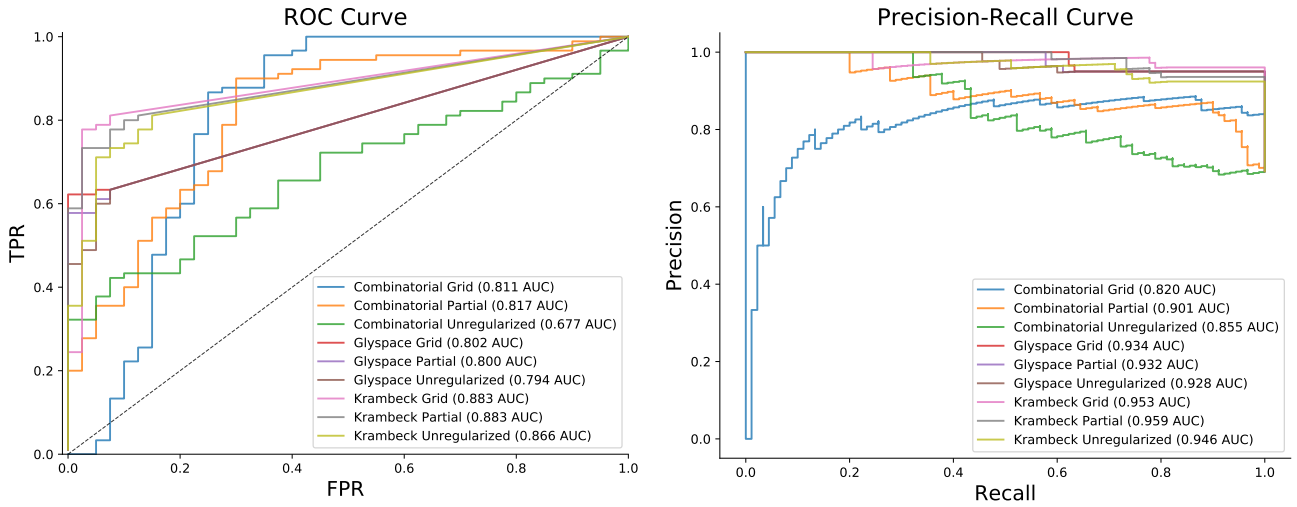

Name	ROC AUC	True Matches [1]	Non-Ambiguous Matches
Combinatorial Unregularized	0.677	86	60
Combinatorial Partial	0.817	87	61
Combinatorial Grid	0.811	87	61
GlySpace Unregularized	0.794	55	48
GlySpace Partial	0.8	55	48
GlySpace Grid	0.802	56	49
Krambeck Unregularized	0.866	70	59
Krambeck Partial	0.883	70	59
Krambeck Grid	0.883	70	59
Yu *et al.* (2013)	-	72[2]	59

[1] Selected at $\phi_o > 5.0$

[2] This count only includes those cases where sufficient MS1 scans were available for a direct comparison

Table 6: Performance Comparison for *Perm-BS-070111-04-Serum*

better performance by defining network connectivity according to enzymatic relationships. This may also alter how the neighborhoods are defined and how $\mathbf{A}$ is parameterized, and in turn how τ is learned. Similarly, this procedure depends upon the scoring functions used, so selecting another set of functions for the data to fit may lead to different parameter values.

Lastly, while these case studies have demonstrated the algorithm's ability to learn network parameters from the data, an expert can define τ and $\mathbf{A}$ themselves or obtain a model fitted on related data and apply it directly without a fitting step. An expert could use this model specification to impose prior beliefs on the evaluation process, and adjust λ to control the importance of the these beliefs. Similarly, one could also use the derivation of $\hat{\phi}_m$ to estimate the score for an unobserved glycan composition, given $\mathbf{A}$ and τ.

5 Conclusions

In this study, we demonstrated the advantages of our application of Laplacian Regularization to smooth LC-MS assignments of glycan compositions across multiple experimental protocols (Hu and Mechref (2012); Khatri *et al.* (2016a)). Our algorithm's performance is competitive with existing tools for analyzing the same type of data, with the added benefit of more flexible evaluation process.

All of the methods demonstrated in this paper are available as part of the open source, cross-platform glycomics and glycoproteomics software `GlycReSoft`, freely available at http://www.bumc.bu.edu/msr/glycresoft/.

References

Akune, Y., Lin, C.-H., Abrahams, J. L., Zhang, J., Packer, N. H., Aoki-Kinoshita, K. F., and Campbell, M. P. (2016). Comprehensive analysis of the N-glycan biosynthetic pathway using bioinformatics to generate UniCorn: A theoretical

N-glycan structure database. *Carbohydrate Research*, **431**, 56–63.

Belkin, M., Niyogi, P., and Sindhwani, V. (2006). Manifold regularization: A geometric framework for learning from labeled and unlabeled examples. *Journal of Machine Learning Research*, **7**(2006), 2399–2434.

Ceroni, A., Maass, K., Geyer, H., Geyer, R., Dell, A., and Haslam, S. M. (2008). GlycoWorkbench: A Tool for the Computer-Assisted Annotation of Mass Spectra of Glycans. *Journal of Proteome Research*, **7**(4), 1650–1659.

Frank, M. and Schloissnig, S. (2010). Bioinformatics and molecular modeling in glycobiology. *Cellular and Molecular Life Sciences*, **67**(16), 2749–2772.

Goldberg, D., Bern, M., North, S. J., Haslam, S. M., and Dell, A. (2009). Glycan family analysis for deducing N-glycan topology from single MS. *Bioinformatics*, **25**(3), 365–371.

Hu, Y. and Mechref, Y. (2012). Comparing MALDI-MS, RP-LC-MALDI-MS and RP-LC-ESI-MS glycomic profiles of permethylated N-glycans derived from model glycoproteins and human blood serum. *Electrophoresis*, **33**(12), 1768–1777.

Hu, Y., Shihab, T., Zhou, S., Wooding, K., and Mechref, Y. (2016). LC-MS/MS of permethylated N-glycans derived from model and human blood serum glycoproteins. *ELECTROPHORESIS*, **37**(11), 1498–1505.

Ichimiya, T., Nishihara, S., Takase-Yoden, S., Kida, H., and Aoki-Kinoshita, K. (2014). Frequent glycan structure mining of influenza virus data revealed a sulfated glycan motif that increased viral infection. *Bioinformatics*, **30**(5), 706–711.

Jaitly, N., Mayampurath, A., Littlefield, K., Adkins, J. N., Anderson, G. A., and Smith, R. D. (2009). Decon2LS: An open-source software package for automated processing and visualization of high resolution mass spectrometry data. *BMC bioinformatics*, **10**(1), 87.

Kaur, P. and O'Connor, P. B. (2006). Algorithms for automatic interpretation of high resolution mass spectra. *Journal of the American Society for Mass Spectrometry*, **17**(3), 459–468.

Kessner, D., Chambers, M., Burke, R., Agus, D., and Mallick, P. (2008). ProteoWizard: Open source software for rapid proteomics tools development. *Bioinformatics*, **24**(21), 2534–2536.

Khatri, K., Klein, J. A., White, M. R., Grant, O. C., Lemarie, N., Woods, R. J., Hartshorn, K. L., Zaia, J., Leymarie, N., Woods, R. J., Hartshorn, K. L., and Zaia, J. (2016a). Integrated omics and computational glycobiology reveal structural basis for Influenza A virus glycan microheterogeneity and host interactions. *Molecular & cellular proteomics : MCP*, **13975**(615).

Khatri, K., Klein, J. A., and Zaia, J. (2016b). Use of an informed search space maximizes confidence of site-specific assignment of glycoprotein glycosylation. *Analytical and Bioanalytical Chemistry*.

Krambeck, F. J. and Betenbaugh, M. J. (2005). A mathematical model of N-linked glycosylation. *Biotechnology and Bioengineering*, **92**(6), 711–728.

Krambeck, F. J., Bennun, S. V., Narang, S., Choi, S., Yarema, K. J., and Betenbaugh, M. J. (2009). A mathematical model to derive N-glycan structures and cellular enzyme activities from mass spectrometric data. *Glycobiology*, **19**(11), 1163–1175.

Kronewitter, S. R., Slysz, G. W., Marginean, I., Hagler, C. D., LaMarche, B. L., Zhao, R., Harris, M. Y., Monroe, M. E., Polyukh, C. A., Crowell, K. L., Fillmore, T. L., Carlson, T. S., Camp, D. G., Moore, R. J., Payne, S. H., Anderson, G. a., and Smith, R. D. (2014). GlyQ-IQ: Glycomics quintavariate-informed quantification with high-performance computing and glycogrid 4D visualization. *Analytical Chemistry*, **86**(13), 6268–6276.

Liu, X., Inbar, Y., Dorrestein, P. C., Wynne, C., Edwards, N., Souda, P., Whitelegge, J. P., Bafna, V., and Pevzner, P. A. (2010). Deconvolution and database search of complex tandem mass spectra of intact proteins: a combinatorial approach. *Molecular & cellular proteomics : MCP*, **9**(12), 2772–2782.

Martens, L., Chambers, M., Sturm, M., Kessner, D., Levander, F., Shofstahl, J., Tang, W. H., Römpp, A., Neumann, S., Pizarro, A. D., Montecchi-Palazzi, L., Tasman, N., Coleman, M., Reisinger, F., Souda, P., Hermjakob, H., Binz, P.-a., and Deutsch, E. W. (2011). mzML–a community standard for mass spectrometry data. *Molecular & cellular proteomics : MCP*, **10**(1), R110.000133.

Maxwell, E., Tan, Y., Tan, Y., Hu, H., Benson, G., Aizikov, K., Conley, S., Staples, G. O., Slysz, G. W., Smith, R. D., and Zaia, J. (2012). GlycReSoft: a software package for automated recognition of glycans from LC/MS data. *PloS one*, **7**(9), e45474.

Peltoniemi, H., Natunen, S., Ritamo, I., Valmu, L., and Räbinä, J. (2013). Novel data analysis tool for semiquantitative LC-MS-MS2 profiling of N-glycans. *Glycoconjugate journal*, **30**(2), 159–70.

Senko, M. W., Beu, S. C., and McLafferty, F. W. (1995). Determination of monoisotopic masses and ion populations for large biomolecules from resolved isotopic distributions. *Journal of the American Society for Mass Spectrometry*, **6**(4), 229–233.

Spiro, M. J. and Spiro, R. G. (2000). Sulfation of the N-linked oligosaccharides of influenza virus hemagglutinin: temporal relationships and localization of sulfotransferases. *Glycobiology*, **10**(11), 1235–42.

Stanley, P., Schachter, H., and Taniguchi, N. (2009). *N-Glycans*. Cold Spring Harbor Laboratory Press.

Tiemeyer, M., Aoki, K., Paulson, J., Cummings, R. D., York, W. S., Karlsson, N. G., Lisacek, F., Packer, N. H., Campbell, M. P., Aoki, N. P., Fujita, A., Matsubara, M., Shinmachi, D., Tsuchiya, S., Yamada, I., Pierce, M., Ranzinger, R., Narimatsu, H., and Aoki-Kinoshita, K. F. (2017). GlyTouCan: an accessible glycan structure repository. *Glycobiology*, **27**(10), 915–919.

Varki, A. (2017). Biological roles of glycans. *Glycobiology*, **27**(1), 3–49.

Yu, C.-Y. C.-Y., Mayampurath, A., Hu, Y., Zhou, S., Mechref, Y., and Tang, H. (2013). Automated annotation and quantification of glycans using liquid chromatography-mass spectrometry. *Bioinformatics*, **29**(13), 1706–1707.

Yu, T. and Peng, H. (2010). Quantification and deconvolution of asymmetric LC-MS peaks using the bi-Gaussian mixture model and statistical model selection. *BMC bioinformatics*, **11**(1), 559.

Zaia, J. (2008). Mass spectrometry and the emerging field of glycomics. *Chemistry & biology*, **15**(9), 881–92.